calculated λ_{max} is in good agreement with existing phthalocyanine optical data.[16b,31]

Conclusions

The results of this investigation demonstrate the wealth of information about quadratic molecular optical nonlinearities which is readily accessible via perturbation theory and the PPP model Hamiltonian. The information includes β tensor components and the frequency dependence thereof, chromophore substituent effects on β, and molecular architecture effects on β. Of course, considerations such as chromophore-laser compatibility (transparency criteria) and the actual number of chromophores that can be packed in a given volume of material ("hyperpolarizability density"[7d]) are also crucial in the design of a frequency-doubling material. The former linear optical information (λ, f) is derived directly from the PPP calculation (or any easily implemented semiempirical calculation), while the latter requires only estimated molecular volumes as additional input. Another advantage of quantum chemical calculation as a prelude to chromophore design and synthesis is realized in the construction of polymeric materials for second harmonic generation. Such materials have been prepared by dispersing an NLO chromophore in a glassy polymer matrix[32] or, more recently, by covalently linking an NLO chromophore to the backbone of a glassy polymer.[9,33] In both cases the requisite noncentrosymmetry of the chromophore arrays is induced by poling above the glass transition temperature in an electric field and then cooling in the electric field. The effectiveness of the poling, in the limit of isolated chromophore molecules, will be directly proportional to the molecular dipole moment.[28a] Hence, being able to evaluate μ_g in advance for a hypothetical chromophore is of obvious benefit in predicting the outcome of the poling experiments.

Acknowledgment. This research was supported by the NSF-MRL program through the Materials Research Center of Northwestern University (Grant DMR85-20280) and by the Air Force Office of Scientific Research (Contract AFOSR-86-0105). We thank Professor G. K. Wong for helpful comments.

(31) Hale, P. D.; Pietro, W. J.; Ratner, M. A.; Ellis, D. E.; Marks, T. J. *J. Am. Chem. Soc.* **1987**, *109*, 5943-5947.

(32) (a) Singer, K. D.; Sohn, J. E.; Lalama, S. J. *Appl. Phys. Lett.* **1986**, *49*, 248-250. (b) Small, K. D.; Singer, K. D.; Sohn, J. E.; Kuzyk, M. G.; Lalama, S. J. in ref 1d, pp 150-169. (c) Meredith, G. A.; Van Dusen, J. G.; Williams, D. J. *Macromolecules* **1982**, *15*, 1385-1389. (d) Hampsch, H. L.; Yang, J.; Wong, G. K.; Torkelson, J. M. *Macromolecules*, in press.

(33) (a) Ye, C.; Marks, T. J.; Yang, J.; Wong, G. K. *Macromolecules* **1987**, *20*, 2322-2324. (b) Ye, C.; Marks, T. J.; Minami, N.; Yang, J.; Wong, G. K. *Mater. Res. Soc. Symp. Series*, in press.

Methyl Radical Formation over Li-Doped MgO. Molecular Orbital Theory

S. P. Mehandru,[†] Alfred B. Anderson,*[†] and James F. Brazdil[‡]

Contribution from the Chemistry Department, Case Western Reserve University, Cleveland, Ohio 44106, and the Research and Development Department, BP America, Inc., 4440 Warrensville Center Road, Warrensville Heights, Ohio 44128. *Received June 22, 1987*

Abstract: Methane adsorption is known to be activated by the presence of chemically formed O^- at the surface of MgO. In the present theoretical study the activation is shown to be the result of the electron accepting ability of O^-. The adsorption of $^{\bullet}CH_3$ formed by $H^{\bullet}$ abstraction is weak and is sensitive to the presence of Mg^{2+} surface, edge, and corner dangling orbitals. The methyl radicals easily desorb, which should allow them to dimerize in the gas phase to form ethane, the main observed reaction product. If there are few O^- in the surface planes, further oxidation via a methoxy intermediate is unlikely, which would be the explanation for the absence of CH_3OH product. We find that adsorbed methyl species can be reoriented at steps because of an attractive σ donation interaction involving a CH σ bond and Mg^{2+} band-gap surface-state orbitals.

It is well established that O^- centers on oxide surfaces possess the ability to cleave CH bonds.[1-10] Active O^- centers have been prepared by a variety of methods, including chemical, γ-irradiation defect formation, cation doping, and charge-transfer excitation from O^{2-} to the empty cation band. The theoretical explanation for this activity lies in the ease with which an electron from a CH bond can reduce the O^- during hydrogen atom abstraction.[11-14] The interaction between O^{2-} and a CH bond is a closed-shell repulsion with a relatively high $H^{\bullet}$ abstraction energy barrier.

Recently Lunsford and co-workers have found that the oxidative dimerization of CH_4 to yield C_2H_4 and C_2H_6 can be achieved in high yield and with good selectivity over Li-promoted MgO catalysts.[8,9] Methyl radicals were produced when CH_4 was passed over MgO at ~500 °C in the presence of O_2.[9,10] Two pathways are believed to be responsible for the radical formation.[9] Over pure MgO, intrinsic cation vacancies react with O_2 to give O^- centers which can abstract $H^{\bullet}$ from CH_4 to produce $^{\bullet}CH_3$(g). For the Li-doped MgO, substitutional Li^+ react with O_2 to form $[Li^+O^-]$ centers which can also bring about $H^{\bullet}$ abstraction from CH_4.

* Address correspondence to this author.
† Case Western Reserve University.
‡ BP America, Inc.

(1) Shvets, V. A.; Vorotyntsev, V. M.; Kazansky, V. B. *Kinet. Katal.* **1969**, *10*, 356.
(2) Kazansky, V. B. *Kinet. Katal.* **1977**, *18*, 43.
(3) Lipatkina, N. I.; Shvets, V. A.; Kazansky, V. B. *Kinet. Katal.* **1978**, *19*, 979.
(4) Kaliaguine, S. L.; Shelimov, B. N.; Kazansky, V. B. *J. Catal.* **1978**, *55*, 384.
(5) Liu, R.-S.; Iwamoto, M.; Lunsford, J. H. *J. Chem. Soc., Chem. Commun.* **1982**, 78.
(6) Liu, H.-F.; Liu, R.-S.; Liew, K. Y.; Johnson, R. E.; Lunsford, J. H. *J. Am. Chem. Soc.* **1984**, *106*, 4117.
(7) Ito, T.; Wang, J.-X.; Lin, C.-H.; Lunsford, J. H. *J. Am. Chem. Soc.* **1985**, *107*, 5062.
(8) Ito, T.; Lunsford, J. H. *Nature (London)* **1985**, *314*, 721.
(9) Driscoll, D. J.; Martir, W.; Wang, J.-X.; Lunsford, J. H. *J. Am. Chem. Soc.* **1985**, *107*, 58.
(10) Driscoll, D. J.; Lunsford, J. H. *J. Phys. Chem.* **1985**, *89*, 4415.
(11) Anderson, A. B.; Ray, N. K. *J. Am. Chem. Soc.* **1985**, *107*, 253.
(12) Mehandru, S. P.; Anderson, A. B.; Brazdil, J. F. *J. Chem. Soc., Faraday Trans. 1* **1987**, *83*, 463.
(13) Mehandru, S. P.; Anderson, A. B.; Brazdil, J. F.; Grasselli, R. K. *J. Phys. Chem.* **1987**, *91*, 2930.

0002-7863/88/1510-1715$01.50/0

Table I. Atomic Orbital Parameters Used in the Calculations (The Text Discusses Their Selection)

atom	orbital	Slater exponent (au)	ionization potential (eV)
Mg	3s	1.279	10.646
	3p	0.979	6.224
O[a]	2s	1.946	26.48
	2p	1.927	11.62
C	2s	1.658	14.59
	2p	1.618	9.26
H[b]	1s	1.2	11.6
H[c]	1s	1.0	11.6

[a] Slater exponents for the oxygens on which the adsorption of fragments is studied are 2.146 and 2.127. [b] For binding to O^-, O^{2-}. [c] For binding to Mg^{2+}.

Table II. Calculated Diatomic Properties with Use of the Atomic Parameters Given in Table I (Dissociation Energies, D_e (eV), and Equilibrium Bond Lengths, R_e (Å))

molecule	D_e	R_e
H_3C–OH	3.46 (~2.9[a])	1.54 (1.43[a])
OH	4.27 (4.62[b])	1.04 (0.97[b])
H_3C–H	5.07 (4.56[a,c])	1.22 (1.10[a])
MgH	2.79 (2.61,[b] 1.43[d])	1.68 (1.73[d])
MgO	4.32 (3.58[d])	1.57 (1.75[d])

[a] *CRC Handbook of Chemistry and Physics*; Weast, R. C., Ed.; CRC Press: Boca Raton, 1986. [b] Rosen, B. *Spectroscopic Data Relative to Diatomic Molecules*; Pergamon: Oxford, 1970. [c] D_0 value. [d] Huber, K. P.; Herzberg, G. *Molecular Spectra and Molecular Structure IV. Constants of Diatomic Molecules*; Van Nostrand: New York, 1979.

The formation and stability of the $[Li^+O^-]$ centers in single-crystal MgO has been extensively studied by Abraham and coworkers.[15-18] These centers were observed following thermal quenching in liquid N_2 of Li-doped MgO crystals that were heated in air or O_2 to high temperatures (~1300 to 1500 K). They were also found to be present in samples subjected to high energy irradiation at low temperatures. The centers formed by heating and quenching are stable up to 750 K whereas those formed by irradiation are unstable at >200 K. A model was proposed[16] to explain these differences. Wang and Lunsford[19] have also recently characterized $[Li^+O^-]$ centers, created by heating and quenching as well as by the irradiation methods, in powder Li-doped MgO catalysts. Both methods resulted in $[Li^+O^-]$ centers that were thermally unstable at >200 K.

In this paper we present the results of a molecular orbital study of CH_4 activation over a cluster model of the (100) surface of MgO. The adsorption of the resulting $^\bullet CH_3$(g) radical is treated. The effects of the $[Li^+O^-]$ centers are modeled simply by reducing the O 2p band population of a large MgO cluster by one electron.

Theoretical Method, Surface Model, and the Electronic Structure of MgO

We employ the atom superposition and electron delocalization molecular orbital (ASED–MO) theory[20] to predict structures, binding energies, and electronic properties in this study. This technique has already been used in several other recent studies involving CH bond activation on oxide[11-14,21] and metal[22] surfaces.

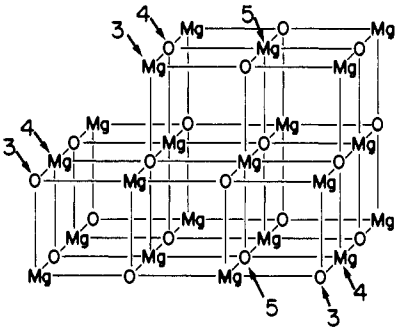

Figure 1. $Mg_{21}O_{20}^{2+}$ cluster used in the calculations. Ions labeled 3, 4, and 5 refer to the respective corner, edge, and face sites discussed in the text.

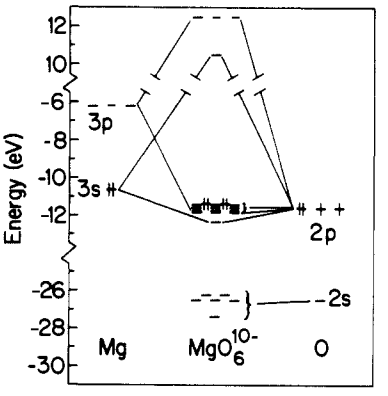

Figure 2. Correlation diagram for MgO_6^{10-}.

The atomic parameters used in all calculations in this paper are in Table I. The 3s Slater exponent for Mg is for the +1 ion and is taken from SCF atomic wave functions.[23] The Mg 3p exponent is set 0.3 au less than the 3s exponent. The Mg 3s ionization potential is experimentally based,[24a] and that for 3p is obtained from the lowest 3s → 3p transition energy for Mg^+.[24b] The 3s and 3p ionization potentials are increased 3 eV to incorporate charge self-consistency in the calculations based on diatomic MgO. The atomic parameters for O, C, and H are the same as used in recent studies.[12,14] Calculated bond energies and lengths for relevant single bonds are given in Table II. All bond lengths given in this paper are variationally optimized to the nearest 0.01 Å and the bond angles to the nearest degree, except where stated otherwise.

MgO is a typical ionic oxide, having a rock-salt structure and a lattice constant of 4.21 Å.[25] Its (100) surface is the natural cleavage plane and contains alternating Mg^{2+} and O^{2-} ions. Both theory[26] and experiment[27] agree that the relaxations in the (100) surface of MgO are small (a few hundreths of an Å) and diminish rapidly with increasing distance from the surface. With this in mind, we have modeled chemisorption with a cluster model which is an idealized rigid truncation of bulk MgO. The $Mg_{21}O_{20}^{2+}$ cluster model used in all our calculations is shown in Figure 1. The 2+ charge assures that all ions are in proper oxidation states

(14) Ward, M. D.; Brazdil, J. F.; Mehandru, S. P.; Anderson, A. B. *J. Phys. Chem.* **1987**, *91*, 6515.
(15) Abraham, M. M.; Chen, Y.; Boatner, L. A.; Reynolds, R. W. *Phys. Rev. Lett.* **1976**, *37*, 839.
(16) Chen, Y.; Tohver, H. T.; Narayan, J.; Abraham, M. M. *Phys. Rev.* **1977**, *B16*, 5535.
(17) Lacy, J. B.; Abraham, M. M.; Boldu, J. L.; Chen, Y.; Narayan, J.; Tohver, H. T. *Phys. Rev.* **1978**, *B18*, 4136.
(18) Boldu, J. L.; Abraham, M. M.; Chen, Y. *Phys. Rev.* **1979**, *B19*, 4421.
(19) Wang, J.-X.; Lunsford, J. H. *J. Phys. Chem.* **1986**, *90*, 5883.
(20) (a) Anderson, A. B. *J. Chem. Phys.* **1975**, *62*, 1187. (b) Anderson, A. B. *J. Chem. Phys.* **1974**, *61*, 4545. (c) Anderson, A. B.; Grimes, R. W.; Hong, S. Y. *J. Phys. Chem.* **1987**, *91*, 4245.
(21) Anderson, A. B.; Ewing, D. W.; Kim, Y.; Grasselli, R. K.; Burrington, J. D.; Brazdil, J. F. *J. Catal.* **1985**, *96*, 222.
(22) (a) Anderson, A. B.; Kang, D. B.; Kim, Y. *J. Am. Chem. Soc.* **1984**, *106*, 6597. (b) Mehandru, S. P.; Anderson, A. B. *J. Am. Chem. Soc.* **1985**, *107*, 844. (c) Kang, D. B.; Anderson, A. B. *J. Am. Chem. Soc.* **1985**, *107*, 7858. (d) Kang, D. B.; Anderson, A. B. *Surf. Sci.* **1985**, *155*, 639. (e) Kang, D. B.; Anderson, A. B. *Surf. Sci.* **1986**, *165*, 221. (f) Anderson, A. B.; Maloney, J. J. *J. Phys. Chem.*, in press.
(23) Clementi, E.; Roetti, C. *Atomic Data and Nuclear Data Tables*; Academic: New York, 1974; Vol. 14.
(24) (a) Lotz, W. *J. Opt. Soc. Am.* **1970**, *60*, 206. (b) Moore, C. E. *Atomic Energy Levels*; National Bureau of Standards Circular 467; U.S. Government Printing Office: Washington, DC, 1958.
(25) Wyckoff, R. W. G. *Crystal Structures*, 2nd ed.; Wiley: New York, 1964; Vol. 2.
(26) (a) Martin, A. J.; Bilz, H. *Phys. Rev. B* **1979**, *19*, 6593. (b) de Wette, F. W.; Kress, W.; Schroder, U. *Phys. Rev.* **1985**, *B32*, 4143.
(27) Welton-Cook, M. R.; Berndt, W. *J. Phys. Chem.* **1982**, *15*, 5691.

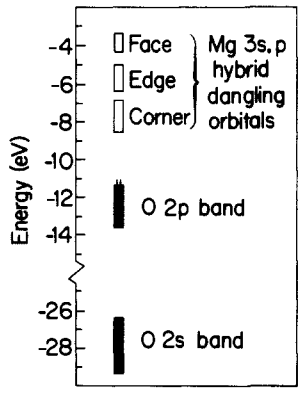

Figure 3. MgO electronic structure calculated by using the $Mg_{21}O_{20}^{2+}$ cluster.

but does not otherwise affect ASED–MO calculations. It has been well established[28-30] that the polycrystalline alkaline-earth oxides outgassed at high temperature have some surface ions with very low coordination numbers (from three to five) which play an important role in catalysis and chemisorption phenomena. Our cluster model consists of surface ions with all possible coordinations, including some step sites. The ions of different coordinations used in the calculations are shown by arrows in Figure 1. The numbers shown with the arrows in Figure 1 represent the coordination number of a particular ion.

With use of a minimal MgO_6^{10-} cluster, the calculated valence electronic structure is illustrated in Figure 2. The highest occupied valence band consists of Mg 3s + 3p and O 2p bonding orbitals having predominant oxygen character, and the O 2p nonbonding orbitals. The empty levels in the conduction band are antibonding between the metal and the oxygens and are mainly metal in character. This picture is qualitatively similar to the Xα calculations of Tossell.[31] The electronic structure obtained by employing the $Mg_{21}O_{20}^{2+}$ cluster model is shown in Figure 3. The empty orbitals corresponding to the coordinatively unsaturated Mg^{2+} ions on the surface are stabilized relative to the bulk Mg^{2+} valence band orbitals and form bands in the bulk band gap. The smaller the coordination number of the surface cation, the smaller is the antibonding destabilization of the empty dangling-bond orbitals, which is why three bands, face, edge, and corner, are predicted to form.

Photoluminescent and reflectance spectra of highly dispersed MgO powders show three optical absorption bands in the range 2.60 to 5.70 eV[32] that are not present in pure single crystals. The luminescence, which is believed to be due to electron-hole pair recombination at the surface, can be quenched by O_2 and H_2.[29] These bands have been proposed to be caused by ions of different low coordination on the surface. Our calculated band gaps between the top of the O 2p band and the bottom of the Mg 3s + 3p corner, edge, and face surface dangling orbital states are 2.8, 5.0, and 7.0 eV, respectively. Thus there is qualitative agreement between experiment and our calculations regarding the position of the empty surface states in MgO.

Methane Activation by O^- Defects on MgO

Our calculations produce a zero activation energy barrier for H• abstraction from CH_4 on the $Mg_{21}O_{20}^{3+}$ cluster model with one hole in the topmost filled level of the O 2p band, which corresponds to one O^- center on the surface of MgO. The geometry of the reaction coordinate for obtaining the activation barrier is the same as in our previous studies of H abstraction from CH_4 by O^{2-} centers in α-Bi_2O_3,[12] and H• abstraction for CH_4 by O^- centers in MoO_3[14] and $CuMoO_4$[14]: C···H···O is linear. The fact that O^- centers are highly reactive even at 77 K[3,33] shows that the barrier should be low. The activation may be easily understood. As soon as a CH bond is brought in line with a surface O^-, a three-center C—H···O σ orbital forms, the antibonding counterpart immediately rises just above the O 2p band, and the hole is transferred to it. The CH bond order then decreases from 1 to $^3/_4$ and the HO bond order increases from 0 to $^1/_4$. With further CH bond stretching the CH σ^* orbital mixes in, which aids the scission. A correlation diagram for H• adding to a surface O^- is shown in Figure 4.

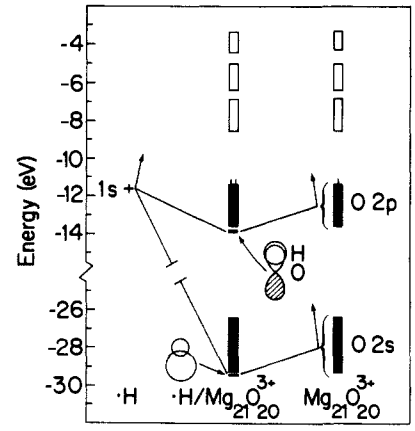

Figure 4. Correlation diagram for H• adsorption to a face O^-.

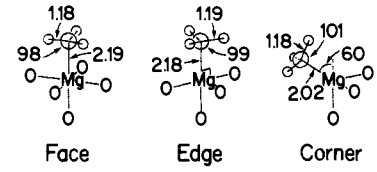

Figure 5. Calculated structures for $^•CH_3$ bonded to various Mg^{2+} sites on the cluster defined in Figure 1.

Table III. Calculated Reaction Energies, ΔE (eV), for the Reductive Heterolytic and the Homolytic Adsorption of Methane Fragments in the Presence of One O^- Radical Anion on the $Mg_{21}O_{20}^{3+}$ Cluster Model

heterolytic mode	ΔE	homolytic mode	ΔE^a
$H^•/O_{3c}^-$, $^•CH_3/Mg_{3c}^{2+}$	−1.85	$H^•/O_{3c}^-$, $^•CH_3/O_{3c}^{2-}$	−1.39, 0.81, 2.84
$H^•/O_{3c}^-$, $^•CH_3/Mg_{4c}^{2+}$	−1.25	$H^•/O_{3c}^-$, $^•CH_3/O_{4c}^{2-}$	−1.48, 0.81, 2.68
$H^•/O_{3c}^-$, $^•CH_3/Mg_{5c}^{2+}$	−1.30	$H^•/O_{3c}^-$, $^•CH_3/O_{5c}^{2-}$	−1.58, 0.59, 2.88
$H^•/O_{4c}^-$, $^•CH_3/Mg_{3c}^{2+}$	−1.69	$H^•/O_{4c}^-$, $^•CH_3/O_{3c}^{2-}$	−1.23, 0.97, 3.00
$H^•/O_{4c}^-$, $^•CH_3/Mg_{4c}^{2+}$	−1.09	$H^•/O_{4c}^-$, $^•CH_3/O_{4c}^{2+}$	−1.32, 0.97, 2.84
$H^•/O_{4c}^-$, $^•CH_3/Mg_{5c}^{2+}$	−1.14	$H^•/O_{4c}^-$, $^•CH_3/O_{5c}^{2-}$	−1.42, 0.75, 3.04
$H^•/O_{5c}^-$, $^•CH_3/Mg_{3c}^{2+}$	−1.68	$H^•/O_{5c}^-$, $^•CH_3/O_{3c}^{2-}$	−1.22, 0.98, 3.01
$H^•/O_{5c}^-$, $^•CH_3/Mg_{4c}^{2+}$	−1.08	$H^•/O_{5c}^-$, $^•CH_3/O_{4c}^{2-}$	−1.31, 0.98, 2.85
$H^•/O_{5c}^-$, $^•CH_3/Mg_{5c}^{2+}$	−1.13	$H^•/O_{5c}^-$, $^•CH_3/O_{5c}^{2-}$	−1.41, 0.76, 3.05

[a] The three numbers are the calculated reaction energies when the methyl radical electron is promoted to the lowest surface state orbital belonging to the corner, the edge, and the face Mg^{2+} cation, respectively.

Table IV. Calculated Reaction Energies, ΔE (eV), for the Formation of a Surface Hydroxyl and Gas-Phase Methyl Radical from Methane Using the $Mg_{21}O_{20}^{3+}$ Cluster Model (One O^- Is Present on the Surface)

reaction	ΔE
$O_{3c}^-(s) + CH_4(g) \rightarrow OH^-(s) + ^•CH_3(g)$	−0.28
$O_{4c}^-(s) + CH_4(g) \rightarrow OH^-(s) + ^•CH_3(g)$	−0.11
$O_{5c}^-(s) + CH_4(g) \rightarrow OH^-(s) + ^•CH_3(g)$	−0.11

The $^•CH_3$ generated from the activation of CH_4 by O^- can either react with the surface Mg^{2+} or O^{2-} or depart into the gas phase. We have calculated the adsorption energies of H• and CH_3• on the 3-, 4-, and 5-coordinated O^- and Mg^{2+} centers, respectively. On the basis of these adsorption energies and the calculated CH

(28) Zecchina, Z.; Stone, F. S. *J. Chem. Soc., Faraday Trans. 1*, **1976**, *72*, 2364.
(29) Coluccia, S.; Deane, A. M.; Tench, A. J. *J. Chem. Soc., Faraday Trans. 1* **1978**, *74*, 2913.
(30) Coluccia, S.; Barton, A.; Tench, A. J. *J. Chem. Soc., Faraday Trans. 1* **1981**, *77*, 2203.
(31) Tossell, J. A. *J. Phys. Chem. Solids* **1975**, *36*, 1273.
(32) Coluccia, S.; Tench, A. J. *J. Chem. Soc., Faraday Trans. 1* **1979**, *75*, 1769 and references therein.
(33) Taarit, Y. B.; Lunsford, J. H. *Chem. Phys. Lett.* **1973**, *19*, 348.

Table V. Calculated Adsorption Energies, E_{ads} (eV), for Methyl Species on Various Coordinatively Unsaturated Sites of the $Mg_{21}O_{20}^{2+}$ Cluster Model

	E_{ads}[a]		
bond	face	edge	corner
$^{\bullet}CH_3/Mg^{2+}$	1.02	0.97	1.57
$^{\bullet}CH_3/O^{2-}$	1.30,[b] −0.87,[c] −3.16[d]	1.20,[b] −1.09,[c] −2.96[d]	1.11,[b] −1.09,[c] −3.12[d]

[a] Negative entries indicate instability; in these cases the same structures as for the stable species were used. [b] Adjacent corner Mg^{2+}. [c] Adjacent edge Mg^{2+}. [d] Adjacent face Mg^{2+}.

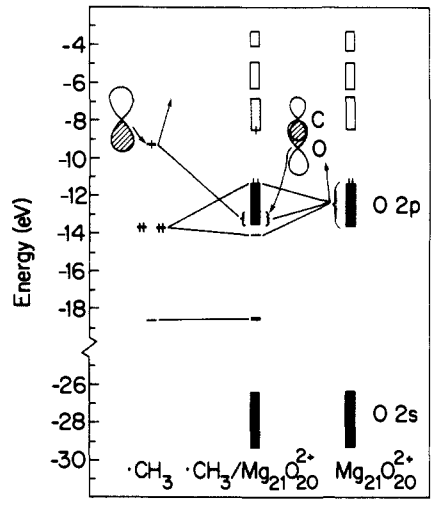

Figure 6. Correlation diagram for $^{\bullet}CH_3$ adsorption to a face O^{2-}.

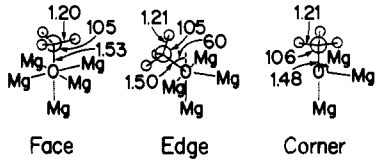

Figure 7. Calculated structures for $^{\bullet}CH_3$ bonded to various O^{2-} sites on the cluster defined in Figure 1.

bond strength in $CH_4(g)$, we derive the reaction energies for the following three possibilities:

$$O^-(s) + O^{2-}(s) + CH_4(g) \rightarrow OH^-(s) + OCH_3^-(s) + e^-$$

$$O^-(s) + Mg^{2+}(s) + CH_4(g) \rightarrow OH^-(s) + Mg^{2+}{}^{\bullet}CH_3(s)$$

$$O^-(s) + CH_4(g) \rightarrow OH^-(s) + {}^{\bullet}CH_3(g)$$

The first two equations represent respectively homolytic and what we term "reductive heterolytic" (or simply "heterolytic") methane adsorption. The third shows the formation of surface OH^- and $^{\bullet}CH_3(g)$. The calculated reaction energies are given in Tables III and IV.

Heterolytic adsorption ($H^{\bullet}$ on O^- and $^{\bullet}CH_3$ on Mg^{2+}) is calculated to be stable for all sites of our cluster model, but the most stable products are obtained when the fragments chemisorb on neighboring corner sites. Figure 5 shows the $^{\bullet}CH_3$ structures on face, edge, and corner sites. The barrier to migration of $^{\bullet}CH_3$ from the corner to the face Mg^{2+} site is ~0.5 eV, based on the adsorption energies of $^{\bullet}CH_3$ on Mg^{2+} sites given in Table V. Once on the face, we calculate a barrier of ~0.7 eV for the diagonal motion of $^{\bullet}CH_3$ between cube face Mg^{2+} sites. This suggests $^{\bullet}CH_3$ could be mobile on the surface of MgO, especially at high temperatures (~500 °C) employed for studying methane oxidation, which may open up a route to dimerization on the surface. On the basis of our calculations, some $^{\bullet}CH_3(g)$ is expected to form directly since the reaction is approximately energy neutral and the transition state is linear. This would open up the possibility of gas-phase dimerization at low temperatures. Alternatively, if some $^{\bullet}CH_3$ adsorbs, at high temperatures it will desorb and dimerize.

Homolytic adsorption on oxygen sites following $H^{\bullet}$ abstraction by O^- is calculated to be stable only if there is a neighboring corner Mg^{2+} ion which can take the radical electron that is promoted when the C–O bond forms (see Figure 6). The calculated reaction energies for all homolytic adsorption possibilities are given in Table III; Figure 7 shows the predicted $^{\bullet}CH_3$ structures at face, edge, and corner sites. In the homolytic case binding of $^{\bullet}CH_3$ to the surface is weakened by the promotion of the electron to a Mg^{2+} surface orbital and in the heterolytic case the C–Mg bond is weak because it holds only one electron (Figure 8). These energies are all summarized in Table V.

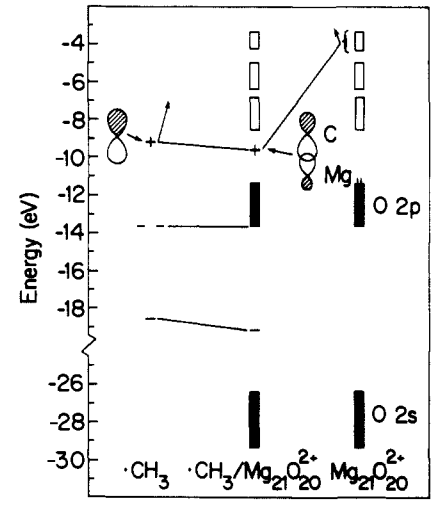

Figure 8. Correlation diagram for $^{\bullet}CH_3$ adsorption to a face Mg^{2+}.

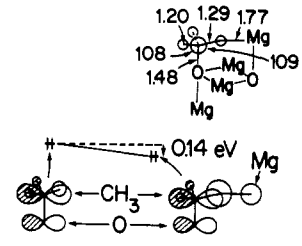

Figure 9. Stabilization of a CH σ orbital causing the $^{\bullet}CH_3$ to reorient when bonded to O^{2-} at the base of a corner Mg^{2+}.

In step locations, the possibility of multiple CH interactions with step atoms must be considered. We have modeled two such cases on the cluster given in Figure 1. When $^{\bullet}CH_3$ binds to the four-coordinate edge Mg^{2+} there is no interaction with the upper edge. When it binds to the corner O^{2-} it reorients so that a CH bond donates into a corner Mg^{2+} dangling surface orbital as shown in Figure 9. At low temperatures such interactions are expected to be observable in vibrational studies on powder samples. Despite the weakening of the CH bond, this structure will be ineffective for activation because the formation of formaldehyde would reduce the surface by two electrons, which is a high-energy process.

Conclusions

The barrier of $H^{\bullet}$ abstraction from CH_4 by O^{2-} sites on the surface of stoichiometric MgO is high because in the initial stages the interaction is a closed-shell repulsion between the CH σ bond electron pair and the O^{2-} lone pair. When O^- is present on the surface the activation energy is very low because one of the CH bond pair electrons reduces the O^- hole and the initial interaction is no longer a closed-shell repulsion. From a molecular orbital perspective, as the transition state is approached a CH σ to O lone pair 3-center σ bond forms along with its antibonding counterpart.

This latter orbital is doubly occupied in the case of O^{2-}, but in the case of O^- it loses an electron to form O^{2-} and becomes only half-filled:

$$H_3C{:}H(g) + {:}\dot{O}{:}^- + Mg^{2+} \longrightarrow {:}\ddot{O}{:}H^- + Mg^{2+}{\cdot}CH_3 \longrightarrow \text{dimerization}$$

or

$$H_3C{:}H(g) + {:}\dot{O}{:}^- \longrightarrow {:}\ddot{O}{:}H^- + {\cdot}CH_3(g) \longrightarrow \text{dimerization}$$

and in either case the activation energy is low.

Heterolytic CH_4 adsorption (H^+ on O^-, $^{\bullet}CH_3$ on Mg^{2+}) is found to be stable relative to the cluster plus $CH_4(g)$, irrespective of the coordination of the Mg^{2+} to which the $^{\bullet}CH_3$ binds, the most stable configuration being the one in which both fragments are adsorbed on the 3-coordinated corner ions. Homolytic CH_4 adsorption ($H^{\bullet}$ on O^-, $^{\bullet}CH_3$ on O^{2-}) is stable only when $^{\bullet}CH_3$ adsorbes adjacent to a corner Mg^{2+} because only in this case is the cation dangling-bond orbital which takes the promoted electron sufficiently stable. We calculate a low barrier to mobility for $^{\bullet}CH_3$ on the face Mg^{2+} sites. Considering that the binding energy of $^{\bullet}CH_3$ on the face Mg^{2+} sites is only $\sim$1 eV (see Table V), the calculations favor its desorption at high temperatures, leading to C_2H_6 formation in the gas phase.

A key question still remaining is why MgO produces different reaction products from $^{\bullet}CH_3$ radicals than does MoO_3. As discussed above, O^- sites on MgO, generated by the presence of the Li^+ dopant, activate CH_4 to form $^{\bullet}CH_3$ which in turn form C_2H_6 as the principal selective oxidation product. On MoO_3, CH_4 activated by O^- centers is selectively oxidized primarily to CH_3OH and CH_2O.[5,6,13] There are two prima facie explanations that come to mind. Since MoO_3 possesses more labile lattice oxygen than MgO and is more easily reduced, oxygen addition to the methyl fragment might occur on MoO_3, which would lead to the oxygenated products, but not on MgO, where $^{\bullet}CH_3$ desorption and dimerization takes place. Another factor of potential importance for answering the above question is the distribution of O^- centers at the surfaces of the two oxides. Wang and Lunsford[19] conclude that most of the $[Li^+O^-]$ centers are not on the surface of MgO and suggest there could be an equilibrium of the form

$$[Li^+O^-]\text{bulk} + O^{2-}\text{surface} \rightleftarrows [Li^+O^{2-}]\text{bulk} + O^-\text{surface}$$

so that the low concentration of surface O^- would explain the selectivity toward C_2H_6 and C_2H_4 formation on this oxide. As discussed in a previous paper,[13] $^{\bullet}CH_3$ can be strongly trapped on O^-, forming methoxy with a strong C–O bond, which would lead to oxygenated products.

Registry No. MgO, 1309-48-4; MeH, 74-82-8; Me, 2229-07-4; H_2, 1333-74-0.

Asymmetric Nitrogen. 67. Geminal Systems. 41. Chiroptical Properties of *N*-Chloro and *N*-Bromo Derivatives of Three-Membered Nitrogen Heterocycles: Aziridines and Diaziridines[1]

G. V. Shustov, G. K. Kadorkina, R. G. Kostyanovsky,* and A. Rauk[2]

Contribution from the Institute of Chemical Physics, Academy of Sciences of the U.S.S.R., Moscow, U.S.S.R., and the Department of Chemistry, The University of Calgary, Calgary, Canada T2N 1N4. *Received July 21, 1987*

Abstract: An experimental and theoretical investigation of the chiroptical properties of *N*-haloaziridines and -diaziridines is described. The following compounds were synthesized and measured: (1*R*,2*S*)- and (1*S*,2*S*)-1-chloro-2-methylaziridine (**1a** and **1b**), the 2,2-dimethyl analogue (+)-(*S*)-**2**, the methyl esters of (1*R*,2*S*)-1-chloro- and (1*R*,2*S*)-1-bromoaziridine-2-carboxylic acid (**3** and **4**), (1*R*,5*S*,6*R*)-*exo*-6-chloro-5-methyl-1,6-diazabicyclo[3.1.0]hexane (**5**), *endo*- and *exo*-6-chloro-5-trifluoromethyl-1,6-diazabicyclo[3.1.0]hexane (**6a** and **6b**), (1*R*,5*R*,6*S*)-*endo*- and (1*R*,5*R*,6*R*)-*exo*-6-chloro-1,6-diazabicyclo[3.1.0]hexane-5-carboxylic acid methyl ester (**7a** and **7b**), the 6-bromo analogue of **7b**, namely **8**, and the methylamides of (1*S*,5*S*,6*S*)-*exo*-6-chloro- and -6-bromo-1,6-diazabicyclo[3.1.0]hexane-5-carboxylic acid (**9** and **10**). The geometries of **1a** and **1b** as well as the parent (1*S*,2*R*)- and (1*S*,2*S*)-1-chlorodiaziridine (**11a** and **11b**) were determined by Hartree–Fock SCF calculations by using a 6-31G* basis set. Excitation energies, oscillator strengths, and optical rotatory strengths were computed directly from CI wave functions for the lower singlet states. The lower electronic transitions of both *N*-chloroaziridines and -diaziridines are to valence states described by π^*_{NCl}–σ^*_{NCl} and n_{NNCl}–σ^*_{NCl}, respectively, where π^*_{NCl} and n_{NNCl} are linear combinations of the nonbonded electrons on the heteroatoms and are the HOMO of the respective systems. The long wavelength Cotton effect (CE) of **1a** and **1b** which differ in configuration at the halogenated nitrogen atom have the same sign, negative. The polar carbomethoxy group of **3** has the opposite effect to a methyl group on the first CE of trans *N*-haloaziridines. Theory predicts that the first CE transition of *N*-chlorodiaziridines will change sign upon inversion of configuration at the nonhalogenated nitrogen atom but not on the configuration of the halogenated nitrogen atom. This result is not observed in comparison of the CD spectra of either **6a**,**6b** or **7a**,**7b**. The theoretical and experimental results can be reconciled if the polar groups (CF_3 or CO_2Me) which are also present interfer in the endo(cis) isomers. The signs of the first CE of all of the exo(trans) *N*-halodiaziridine derivatives agree with the theoretical results on **11b**.

Secondary *N*-halogenamines (R_2N-Hal, Hal = Cl, Br) are readily synthesized; they are characterized by an absorption maximum in the accessible region of the UV spectrum.[3,4] Therefore it is interesting to use a halogenamino group as an asymmetrically disturbed chromophore for studying the stereochemistry of chiral amines by chiroptical methods.[5-11] For usual *N*-halogenamines, a low inversion barrier of the nitrogen atom

* Address correspondence to this author at The University of Calgary.

(1) Previous papers in this series: Shustov, G. V.; Denisenko, S. N.; Shibaev, A. Yu.; Puzanov, Yu, V.; Kostyanovsky, R. G. *Khim. Fisica* **1988**, in press. (b) Shustov, G. V.; Denisenko, S. N.; Shibaev, A. Yu.; Puzanov, Yu. V.; Romero Maldonado, I. K. A.; Kostyanovsky, R. G. *Izvest. Akad. Nauk SSSR, Ser. Khim.* **1988**, in press.

0002-7863/88/1510-1719$01.50/0